Comparative developmental transcriptomics of *Drosophila* mushroom body neurons highlights the mevalonate pathway as a regulator of axon growth

Lora Fahdan[1,2], Hagar Meltzer[1,2], Noa Wigoda[3], Ron Rotkopf[3], Oren Schuldiner [1,2*]

[1] Department of Molecular Cell Biology, Weizmann Institute of Science, Rehovot, Israel
[2] Department of Molecular Neuroscience, Weizmann Institute of Science, Rehovot, Israel
[3] Bioinformatics unit, Department of Life Sciences Core Facilities, Weizmann Institute of Science, Rehovot, Israel

[*] Correspondence to: oren.schuldiner@weizmann.ac.il

Abstract

The ability of neurons to extend axons is governed by tightly regulated genetic programs that vary across developmental stages and cell types. Understanding the molecular features that control axon growth potential is critical for uncovering how neural circuits form, mature, and respond to injury or disease. The *Drosophila* mushroom body (MB) offers a powerful model to dissect axon growth programs, as lineage-related Kenyon cells (KCs) undergo different developmental events under shared spatiotemporal conditions. During metamorphosis, γ-KCs undergo axon pruning, followed by developmental regrowth at the same time-frame as α/β-KCs initiate axon growth - thus providing a unique opportunity to compare these distinct growth paradigms. To uncover the underlying genetic programs, we performed RNA-sequencing of α/β- and γ-KCs during their initial growth and developmental regrowth, respectively, revealing dynamic transcriptional changes and identifying 300 shared genes upregulated during both growth states. A targeted loss-of-function screen revealed genes specifically required for either α/β initial growth, γ regrowth, or both. Focusing on one such candidate, Pmvk, we found that it plays a crucial role in axon regrowth by acting within the mevalonate pathway. Notably, other enzymes in this pathway were also required, suggesting that the entire metabolic pathway is essential for supporting regrowth. Using mutant analyses and rescue exepriements, we demosntrate that Pmvk likely controls axon regrwoth via prenylation of Rheb, an effector of the TOR pathway, which we previously found to be required for regrowth. Our developmental transcriptomic atlas not only advances understanding of intrinsic axon growth programs, but also provides candidate genes and a valuable framework for future studies aimed at enhancing axon regeneration in the adult nervous system.

Introduction

Axon growth is essential for correct circuit formation during development. It is a tightly controlled process, and an emerging paradigm claims that axon growth and synaptogenesis are mutually exclusive processes (Hilton et al., 2022). Despite its significance, the cellular and molecular mechanisms that govern different axon growth states are not fully understood. Axon growth capacity is also crucial during regeneration following injury. Santiago Ramon y Cajal (Rozo et al., 2024) first noted that while the adult mammalian central nervous system typically fails to regenerate, the peripheral nervous system can sprout and grow new connections. Regeneration is influenced by both intrinsic factors that determine axon growth potential, and extrinsic factors such as deposits by glia or other cells (Qian and Zhou, 2020; Sutherland and Geoffroy, 2020). Therefore, understanding how intrinsic axon growth capacity is mechanistically regulated in different developmental contexts should also forward our understanding of what limits axon regeneration in pathological states such as spinal cord injury.

Drosophila is an excellent model organism to investigate axon growth potential in different developmental contexts, due to its unparalleled neurogenetic toolkit combined with the extensive remodeling of its nervous system during metamorphosis. Neuronal remodeling is a conserved strategy to refine neural circuits, by eliminating exuberant connections and promoting regrowth toward adult-specific targets (Schuldiner and Yaron, 2015). The *Drosophila* mushroom body (MB), a center of associative learning and memory in the fly brain (Belle and Heisenberg, 1994), undergoes stereotypic remodeling during early pupal stages. The MB is comprised of three major types of intrinsic neurons: the γ-, α′/β′- and α/β-Kenyon Cells (KCs; Lee et al., 1999), sequentially born from four neuroblasts per hemisphere. The first-born γ-KCs initially extend axons that bifurcate to form the larval vertical and medial lobes. However, in early pupae (initiated at ~6 hours after puparium formation; h APF), both axonal lobes are pruned back to their branch point, followed by axon regrowth (initiated at ~24h APF) to form the adult-specific γ lobe that only projects medially (Lee et al., 1999). In contrast, the later-born α′/β′- and α/β-KCs retain their original bifurcated projections into adulthood (Figure 1A). Importantly, the initial growth of α/β-axons occurs at ~24h APF – the same time in which γ-axons initiate developmental regrowth.

γ-axons thus undergo dynamic transitions between intial growth, pruning, and regrowth, all of which were shown to be tightly regulated by nuclear receptor complexes (Lee et al., 2000;Rabinovich et al., 2016; Yaniv et al., 2012), implying they are goverened by genetic programs. We previously employed RNA-sequencing to characterize the transcriptional landscape of γ-KCs throughout development at high temporal resolution (Alyagor et al., 2018). Moreover, our lab demonstrated that the molecular mechanisms underyling developmental regrowth are distinct from those of initial axon growth, yet show similarities to regeneration after injury (Marmor-Kollet and Schuldiner, 2016; Rabinovich et al., 2016; Sudarsanam et al., 2020; Yaniv et al., 2020, 2012). The fact that different axon growth states share core machinery yet also show distinct pathways depending on the cellular and developmental context, motivated us to directly compare the genetic programs of initial axon growth and developmental axon regrowth.

In this study, we took advantage of the temporal overlap between α/β initial growth and γ regrowth to compare the transciptional landscape of these distinct axon growth programs occuring in a similar developmental, environmental and lineage context (Figure 1A-B). This comparison laid the groundwork for a large-scale loss-of-function screen aimed at uncovering genes and pathways required for both axon growth paradigms. Through this approach, we identified 12 genes that are required for axon growth and/or regrowth. We delved deeper into phosphomevalonate kinase (Pmvk), an enzyme in the mevalonate pathway, and found that it likely promotes axon regrowth, but not initial growth, at least in part via the TOR pathway. Together, our findings reveal shared and divergent molecular pathways underlying distinct axon growth programs, offering new insights into how intrinsic factors shape neuronal growth capacity. By combining time-course transcriptional profiling of defined neuronal populations with functional genetics, we not only uncovered key regulators of axon regrowth, but also provide a rich, publicly available dataset that can serve as a foundation for future discoveries in neuronal development.

139 **Methods**

140 **Key Resources Table**

REAGENT or RESOURCE	SOURCE	IDENTIFIER
Antibodies		
Chicken anti GFP 1:500	AVES	Cat#GFP-1020; RRID: AB_10000240
Mouse monoclonal anti FasII 1:25	Developmental Studies Hybridoma Bank (DSHB)	Cat#1D4; RRID:AB_528235
Mouse monoclonal anti dac 1:10	Developmental Studies Hybridoma Bank (DSHB)	Cat#mAbdac2-3;RRID: AB_528190
Goat anti mouse Alexa fluor 647 1:300	Invitrogen	Cat#A32728; RRID:AB_2633277
FITC Goat anti Chicken 1:300	Invitrogen	Cat#16055;RRID: AB_2534728
Chemicals, Peptides, and Recombinant Proteins		
Cell Dissociation Solution	Sigma Aldrich	Cat# C1544
Collagenase/dispase mix	Roche	Cat# 10269638001
Critical Commercial Assays		
Pico pure RNA isolation kit	Life Technologies	Cat# KIT0204
Deposited Data		
Raw data files for Developmental seq	NCBI Gene Expression Omnibus	GEO: GSE308165
Experimental Models: Organisms/Strains		
w[1118];P{y[+t7.7]w[+mC]=GMR16B01GAL4}attP2	BDSC	48712
w[1118];P{y[+t7.7]w[+mC]=GMR71G10GAL4}attP2	BDSC	39604
w[*];P{y[+t7.7]w[+mC]=10XUASIVSmCD8::GFP}attP2	BDSC	32185
y[1]w[1118];P{w[+mC]=QUASmtdTomato3xHA}14/CyO	BDSC	30004

GMR71G10-QF2 (2nd Chromosome)	(Bornstein et al., 2015)	N/A
y[1]sc[*]v[1]sev[21];P{y[+t7.7]v[+t1.8]=TRiP.HMS00991}attP2 (UAS-emb RNAi)	BDSC	34021
y[1]sc[*]v[1]sev[21];P{y[+t7.7]v[+t1.8]=TRiP.HMS00347}attP2 (UAS-mira RNAi)	BDSC	32356
y[1]sc[*]v[1]sev[21];P{y[+t7.7]v[+t1.8]=TRiP.HMS00487}attP2 (UAS-chm RNAi)	BDSC	32484
y[1]sc[*]v[1]sev[21];P{y[+t7.7]v[+t1.8]=TRiP.HMC03533}attP2 (UAS-beag RNAi)	BDSC	53306
y[1]sc[*]v[1]sev[21];P{y[+t7.7]v[+t1.8]=TRiP.HMS01281}attP2 (UAS-CCT7 RNAi)	BDSC	34931
y[1]sc[*]v[1]sev[21];P{y[+t7.7]v[+t1.8]=TRiP.HMS05732}attP40 (UAS-twr RNAi)	BDSC	67881
y[1]sc[*]v[1]sev[21];P{y[+t7.7]v[+t1.8]=TRiP.HMS02380}attP2 (UAS-CadN RNAi)	BDSC	41982
y[1]v[1];P{y[+t7.7]v[+t1.8]=TRiP.HMS00909}attP2 (UAS-Bap60 RNAi)	BDSC	33954
y[1]v[1];P{y[+t7.7]v[+t1.8]=TRiP.GL01246} attP2 (UAS-CCT5 RNAi)	BDSC	41818
y[1]v[1];P{y[+t7.7]v[+t1.8]=TRiP.HMJ21725}attP40 (UAS-Hsp67Ba RNAi)	BDSC	53007
y[1]v[1];P{y[+t7.7]v[+t1.8]=TRiP.HMJ21488}attP40 (UAS-Dip-B RNAi)	BDSC	54045
y[1]v[1];P{y[+t7.7]v[+t1.8]=TRiP.HMJ21057}attP40/CyO (UAS-Pmvk RNAi)	BDSC	50955
P{hsFLP}1y[1]w[1118];P{HD_CFD00252}attP40/CyO-GFP (Pmvk gRNA)	VDRC	341218
Pmvk E20*/Cyo	This study	N/A
y[1]v[1];P{y[+t7.7]v[+t1.8]=TRiP.HMJ22759}attP40 (UAS-Mvk RNAi)	BDSC	60442
P{KK101807}VIE-260B (UAS-hmgcr RNAi)	VDRC	108617
P{w[+mC]=UAS-Dcr-2.D}1	BDSC	24648
P{KK105673}VIE-260B (UAS-GGT1 RNAi)	VDRC	110288
y[1]v[1];P{y[+t7.7]v[+t1.8]=TRiP.HMJ21755}attP40 (UAS-Fntb RNAi)	BDSC	53029
y[1]sc[*]v[1]sev[21];P{y[+t7.7]v[+t1.8]=TRiP.GL01026}attP2 (UAS-FntaRNAi)	BDSC	36873
y[1]v[1];P{y[+t7.7]v[+t1.8]=TRiP.HMC03386} attP40 (UAS-Dhdds RNAi)	BDSC	51815

y[1]v[1];P{y[+t7.7]v[+t1.8]=TRiP.HMC03486} attP40 (UAS-Pdss2 RNAi)	BDSC	51910
w[1118]P{GD4696}v47001 (UAS-qm RNAi)	VDRC	47001
w[1118];P{w[+mC]=UAS-S6k.STDETE}2 (UAS-S6K^{CA})	BDSC	6914
w[*];P{w[+mC]=UAS-Rheb.Pa}3 (UAS-Rheb)	BDSC	9689
w[*];P{w[+mC]=UAS-Rho1.V14}2.1/TM6 (UAS-Rho)	BDSC	8144
y[1]v[1];P{y[+t7.7]v[+t1.8]=UASLUC.VALIUM10}attP2 (UAS- Luciferase)	BDSC	35788
Primers used for Pmvk mutation screening:	This study	N/A
TAAACACAACAGGCCGCAGT		
AATAGAGCTTGTGTGGCGGT		
Software and Algorithms		
Partek software		
DEseq2	Love et al. (2014)	N/A
STAR	(Dobin et al., 2013)	N/A
FIJI	Image J	https://imagej.net/Fiji/Downloads
Other		
NovaSeq6000 instrument (Illumina)	Illumina	N/A
BD FACSAriaIII	BD Bioscience	N/A
Zeiss LSM 800 and 980 confocal microscope	Zeiss	N/A

141

142 **Fly husbandry and strains**

143 All fly strains were reared at 25°C (unless indicated otherwise) under standard laboratory
144 conditions on molasses-containing food. Unless specifically written, similar numbers of
145 male and female flies were taken. 'Adult' refers to flies 3-5 days post eclosion.
146 The 30 driver lines used to specifically label α/β-KCs are described in Supplementary
147 Table 1. The RNAi lines used in the loss-of-function screen are detailed in Supplementry
148 Table 2.

149 RNAi lines were obtained from the Vienna Drosophila RNAi Center (VDRC), Austria, or
150 from Bloomington Drosophila Stock Center (BDSC), USA.
151 **Genotypes**
152 hsFLP is y,w,hsFLP122; 40A and 82B are FRTs on 2L and 3R respectively; 71G10 is
153 GMR71G10-GAL4; 71G10-QF2 is GMR71G10-QF2; OK107 is OK107-GAL4; R44E04 is
154 GMR44E04-GAL4; 16B01 is GMR16B01-Gal4; G80 is TubP-Gal80. QUAS-mtdT is
155 QUAS-mtdt:HA, UAS-CD8:GFP is UAS-mCD8::GFP.
156 Males and females were used interchangeably.
157 Figure1:
158 (C) UAS-CD8:GFP/+ ; 71G10/+
159 (D) UAS-CD8:GFP/+ ; 16B01/+
160 Figure3:
161 (B) 71G10-QF2, QUAS-mtdT/+ ; UAS-Luciferase/+ ; OK107/+
162 (D) 71G10-QF2, QUAS-mtdT/+ ; UAS-beag RNAi$^{TRiP.HMC03533}$/+ ; OK107/+
163 (E) 71G10-QF2, QUAS-mtdT/+ ; UAS-chm RNAi$^{TRiP.HMS00487}$/+ ; OK107/+
164 (F) 71G10-QF2, QUAS-mtdT/+ ; UAS-Hsp67Ba RNAi$^{TRiP.HMJ21725}$/+ ; OK107/+
165 (H) 71G10-QF2, QUAS-mtdT/+ ; UAS-CCT5 RNAi^{HMC02988}/+ ; OK107/+
166 (I) 71G10-QF2, QUAS-mtdT/+ ; UAS-CCT7 RNAi$^{TRiP.HMS01281}$/+ ; OK107/+
167 (J) 71G10-QF2, QUAS-mtdT/+ ; UAS-emb RNAi$^{TRiP.GL01246}$/+ ; OK107/+
168 (K) 71G10-QF2, QUAS-mtdT/+ ; UAS-Dip-B RNAi$^{TRiP.HMJ21488}$/+ ; OK107/+
169 (L) 71G10-QF2, QUAS-mtdT/+ ; UAS-Bap60 RNAi$^{TRiP.HMS00909}$/+ ; OK107/+
170 (M) 71G10-QF2, QUAS-mtdT/+ ; UAS-Pmvk RNAi$^{TRiP.HMJ21057}$/+ ; OK107/+
171 (N) 71G10-QF2, QUAS-mtdT/+ ; UAS-twr RNAi$^{TRiP.HMS05732}$/+ ; OK107/+
172 (O) 71G10-QF2, QUAS-mtdT/+ ; UAS-cadN RNAi$^{TRiP.HMS02380}$/+ ; OK107/+
173 (Q) 71G10-QF2, QUAS-mtdT/+ ; UAS-mira RNAi$^{TRiP.HMS00347}$/+ ; OK107/+
174 Figure 4:
175 (A,C) 71G10, UAS-CD8:GFP/+ ; UAS-Luciferase/+
176 (B,D) 71G10, UAS-CD8:GFP/+ ; UAS- Pmvk RNAi $^{TRiP.HMJ21057}$/+
177 (E) R44E04, UAS-CD8:GFP/+ ; UAS-Luciferase/+
178 (F) R44E04, UAS-CD8:GFP/+ ; UAS- Pmvk RNAi $^{TRiP.HMJ21057}$/+
179 (G,I) hsFLP, UAS-CD8::GFP/+; G80,40A/40A; 71G10/+

180 (H,J)hsFLP,CD8:GFP/+;UAS-PmvkRNAi $^{TRiP.HMJ21057}$(attP40)/+;82B,Gal80/82B;OK107/+

181 (K) hsFLP, UAS-CD8::GFP/+; G80,40A/40A; R44E04/+

182 (L) hsFLP, UAS-CD8::GFP/+; G80,40A/*Pmvk*^{E20*},40A; R44E04/+

183 Figure 5:

184 (A) 71G10-QF2, QUAS-mtdT/+ ; UAS-Luciferase/+ ; OK107/+

185 (B) UAS-Dicer;71G10-QF2, QUAS-mtdT/+ ; UAS-hmgcr RNAi KK 101807/+ ; OK107/+

186 (C) 71G10-QF2, QUAS-mtdT/+ ; UAS-Mvk RNAi $^{TRiP.HMJ22759}$/+ ; OK107/+

187 Figure 6:

188 (C) hsFLP, UAS-CD8::GFP/+; G80,40A/40A; 71G10/+

189 (D) hsFLP, UAS-CD8::GFP/+; G80,40A/*Pmvk*^{E20*},40A; 71G10/+

190 (E) hsFLP, UAS-CD8::GFP/+; G80,40A/*Pmvk*^{E20*},40A; 71G10/UAS-Rho

191 (F) hsFLP, UAS-CD8::GFP/+; G80,40A/*Pmvk*^{E20*},40A; 71G10/UAS-Rheb

192 (G) hsFLP, UAS-CD8::GFP/+; G80,40A/*Pmvk*^{E20*},40A; 71G10/UAS-S6K^{CA}

193 Figures S3:

194 (A) hsFLP,UAS-CD8:GFP;G80,40A/40A; OK107/+

195 (B) hsFLP,UAS-CD8:GFP;G80,40A/40A; UAS-emb RNAi$^{TRiP.HMS00991}$/+; OK107/+

196 (C) hsFLP,UAS-CD8:GFP;G80,40A/40A; UAS-CCT5 RNAi$^{TRiP.GL01246}$/+; OK107/+

197 (D) hsFLP,UAS-CD8:GFP;G80,40A/40A; UAS-CCT7 RNAi$^{TRiP.HMS01281}$/+; OK107/+

198 (E) hsFLP,UAS-CD8:GFP;G80,40A/40A; UAS-CadN RNAi$^{TRiP.HMS02380}$/+; OK107/+

199 (F) hsFLP,CD8:GFP/+;UAS-Pmvk RNAi $^{TRiP.HMJ21057}$/+;82B,G80/82B;OK107/+

200 (G) hsFLP,CD8:GFP/+; UAS-twr RNAi$^{TRiP.HMS05732}$/+;82B,G80/82B;OK107/+

201 (H) hsFLP,UAS-CD8:GFP;G80,40A/40A; UAS-Bap60 RNAi$^{TRiP.HMS00909}$/+; OK107/+

202 (I) hsFLP,CD8:GFP/+; UAS-Dip-B RNAi$^{TRiP.HMJ21488}$ /+;82B,G80/82B;OK107/+

203 (J) hsFLP,UAS-CD8:GFP;G80,40A/40A; UAS-beag RNAi$^{TRiP.HMC03533}$/+; OK107/+

204 (K) hsFLP,UAS-CD8:GFP;G80,40A/40A; UAS-chm RNAi$^{TRiP.HMS00487}$/+; OK107/+

205 (L) hsFLP,CD8:GFP/+; UAS-Hsp67Ba RNAi$^{TRiP.HMJ21725}$ /+;82B,G80/82B;OK107/+

206 (M) hsFLP,UAS-CD8:GFP;G80,40A/40A; UAS-mira RNAi$^{TRiP.HMS00347}$/+; OK107/+

207 Figures S4:

208 (A) hsFLP,UAS-CD8:GFP;G80,40A/40A; OK107/+

209 (B) hsFLP,UAS-CD8:GFP;G80,40A/40A; UAS-emb RNAi$^{TRiP.HMS00991}$/+; OK107/+

210 (C) hsFLP,UAS-CD8:GFP;G80,40A/40A; UAS-CCT5 RNAi$^{TRiP.GL01246}$/+; OK107/+

211 (D) hsFLP,UAS-CD8:GFP;G80,40A/40A; UAS-CCT7 RNAi$^{TRiP.HMS01281}$/+; OK107/

212 Figure S5:

213 (B) 71G10-QF2, QUAS-mtdT/+ ; UAS-Luciferase/+ ; OK107/+

214 (C) UAS-Dicer;71G10-QF2, QUAS-mtdT/+ ; UAS-GGT1 RNAi KK 105673/+ ; OK107/+

215 (D)71G10-QF2, QUAS-mtdT/+ ; UAS-Fntb RNAi $^{TRiP.HMJ21755}$/+ ; OK107/+

216 (E) 71G10-QF2, QUAS-mtdT/+ ; UAS-Fnta RNAi $^{TRiP.GL01026}$/+ ; OK107/+

217 (F) 71G10-QF2, QUAS-mtdT/+ ; UAS-Dhdds RNAi $^{TRiP.HMC03386}$/+ ; OK107/+

218 (G) 71G10-QF2, QUAS-mtdT/+ ; UAS-Pdss2 RNAi $^{TRiP.HMC03486}$/+ ; OK107/+

219 (H) 71G10-QF2, QUAS-mtdT/+ ; UAS-qm RNAi GD 4696/+ ; OK107/+

220 Figure S6:

221 (A) hsFLP, UAS-CD8::GFP/+; G80,40A/40A; 71G10/+

222 (B) hsFLP, UAS-CD8::GFP/+; G80,40A/40A; 71G10/ UAS-Rheb

223 (C) hsFLP, UAS-CD8::GFP/+; G80,40A/40A; 71G10/UAS-Rho

224 (D) hsFLP, UAS-CD8::GFP/+; G80,40A/40A; 71G10/ UAS-S6K^{CA}

225 Figure S7:

226 (A) hsFLP, UAS-CD8::GFP/+; G80,40A/40A; 71G10/+

227 (B) hsFLP, UAS-CD8::GFP/+; G80,40A/*Pmvk*^{E20*},40A; 71G10/+

228 (C) hsFLP, UAS-CD8::GFP/+; G80,40A/*Pmvk*^{E20*},40A; 71G10/UAS-Rho

229 (D) hsFLP, UAS-CD8::GFP/+; G80,40A/*Pmvk*^{E20*},40A; 71G10/UAS-Rheb

230 (E) hsFLP, UAS-CD8::GFP/+; G80,40A/*Pmvk*^{E20*},40A; 71G10/UAS-S6K^{CA}

231 **Materials and Method**

232 **Cell Dissociation and Sorting**

233 Brains were dissected in a cold Ringer's solution and incubated at 29°C with a
234 collagenase/dispase mix for 15 minutes for larval and pupal brains, and 30 minutes for
235 adult brains. After enzymatic digestion, the tissue was washed with a dissociation solution
236 (Sigma-Aldrich) and mechanically dissociated into single cells. The cell suspension was
237 then passed through a 35µm mesh (Falcon) to remove debris and cell clusters. A total of
238 1000 GFP+ cells were sorted using a BD FACSAriaIII (BD Biosciences) equipped with a
239 100µm nozzle under low pressure, directly into 100µl of Pico-Pure RNA isolation kit
240 extraction buffer (Life Technologies). RNA extraction was subsequently performed using
241 the kit, or frozen at -80°C for future use. To minimize potential injury responses, samples

242 were kept on ice throughout the procedure, from dissection to RNA extraction except from
243 the dissociation enzyme incubation.

244 **RNA Amplification and Library Preparation**

245 **Bulk smart-seq2**

246 Bulk RNA-seq libraries were prepared at the Crown Genomics Institute of the Nancy and
247 Stephen Grand Israel National Center for Personalized Medicine (G-INCPM), Weizmann
248 Institute of Science. Libraries were prepared based on the smart-seq2 protocol (Picelli et
249 al., 2014) with small modifications. Briefly, 250 pg of RNA was used as input. Reverse
250 transcription was performed using Oligo-dT primers, followed by PCR (16 cycles). After
251 Agencourt Ampure XP beads cleanup (Beckman Coulter), the amplified cDNA underwent
252 library generation using Nextera XT (Illumina). Libraries were quantified by Qubit (Thermo
253 Fisher Scientific) and TapeStation (Agilent). Sequencing was done on a NovaSeq6000
254 instrument (Illumina) using an SP 100 cycles kit, allocating approximately 13M reads per
255 sample (single read sequencing).

256 **Analysis of RNA-Seq Data**

257 Two sequencing runs of RNA were combined, yielding a mean of 22.5 million reads
258 (single-read sequencing) and a minimum of 10 million reads per sample. The reads were
259 aligned with STAR (DOI: 10.1093/bioinformatics/bts635) v2.5.2 to the reference
260 genome of *Drosophila melanogaster* (DM6, UCSC). Gene annotations were obtained
261 from FlyBase.org (Dmel r6.46). Gene expression levels were quantified using STAR.
262 12,493 genes had been identified in total across the two datasets (in either γ or α/β or
263 both). Out of these, only genes that were expressed in at least four samples (replicates)
264 of a single time point (condition) were kept, so that the 8,221 genes that met this
265 requirement were used in further analysis. To get relevant p-values and fold-changes for
266 comparisons of a condition with all-zeros vs. a condition with non-zero value, zero values
267 were replaced with randomly assigned numbers between 1 and 7. The updated count
268 matrix was subjected to normalization and statistical analysis using the UTAP2 pipeline
269 (Lindner et al., 2025) which took batch effects into account and employed the DESeq2
270 algorithm (Love et al., 2014). Genes were considered differentially expressed if they had
271 an adjusted p-value (padj) ≤ 0.05, a fold change ≥ 1.5 and a mean read counts of ≥10
272 reads.

Clusters and Sub-Clusters Generation and Analysis

Based on the α/β transcriptome, gene expression at each of the five developmental stages (18, 21, 24, 27, and 30 hours APF) was compared to the adult stage. Genes were classified as differentially expressed during development if, at any time point, their expression was at least 1.5-fold different from the adult expression, with an adjusted p-value (padj) < 0.05 and a mean read count of at least 10, resulting in the identification of 3,345 genes. Cluster analysis was performed on the 3,345 genes that showed differential expression in at least one developmental time point (compared to the adult).Using Partek software, we performed k-means clustering on the mean expression across replicates at each developmental time point, selecting k = 8 after testing multiple values, as this produced the most distinct and coherent clusters. For subclustering the α/β Cluster 1 and Cluster 2, we employed k-means clustering based on the average expression of those genes in γ-KCs across replicates at each time point. Cluster 1 was further subdevided into 10 additional subclusters 1A-J, and cluster 2 into 7 subclusters 2A-G. We identified statistically enriched terms using Metascape (Zhou et al., 2019).This tool integrates multiple authoritative databases to identify enriched Gene Ontology (GO) terms, canonical pathways, and functional gene groups. For each cluster, the input gene lists were analyzed against the default background, and significantly enriched categories were reported based on a hypergeometric test with multiple-testing correction. The resulting enrichment networks and bar plots were used to interpret the biological processes and pathways associated with each gene cluster.

Immunohistochemistry

Brains were dissected in Ringer's solution, fixed with 4% paraformaldehyde (PFA) for 20 minutes at room temperature (RT), and subsequently washed in phosphate buffer (PB) containing 0.3% Triton-X (PBT). The washing protocol consisted of three rapid rinses followed by three additional washes, each lasting 20 minutes. To minimize non-specific staining, the samples were incubated in PBT supplemented with 5% heat-inactivated goat serum. They were then treated with primary antibodies overnight at 4°C, followed PBT washes (as above), then incubation with secondary antibodies for 2 hours at RT, followed by PBT washes. The brains were then mounted using SlowFade (Invitrogen) and

303 visualized using Zeiss LSM800 or LSM980 confocal microscopes. Image analysis was
304 carried out with ImageJ 1.51 (NIH).

305 **Generation of CRISPR Mutant Flies**

306 To generate the Pmvk mutant, we used a fly strain (VDRC#341218) that expresses two
307 guide RNAs (sgRNAs) under the control of a UAS promoter. These sgRNAs target coding
308 exons in the 5′ region of the Pmvk gene, without overlapping the start codon. This design
309 facilitates the introduction of small insertions or deletions (indels) in the presence of Cas9.
310 To drive germline mutagenesis, we incorporated a nanos-Gal4 on the third chromosome
311 and crossed these flies with a UAS-Cas9 expressing fly, which also carries a 40A FRT
312 site on the second chromosome. After two generations, individual males were crossed
313 with balancer flies for mutation screening. We recovered a Pmvk mutant allele that
314 contained a nucleotide substitution (G>T) at position 60 ($Pmvk^{E20*}$, Figure 4G).

315 **MARCM analysis**

316 Mosaic Analysis with a Repressible Cell Marker (MARCM) clones were generated in a
317 similar strategy as previously described (Lee and Luo, 1999). To generate γ- or α/β-
318 clones, newly hatched larvae (NHL) or pupae at 0 h APF, respectively, underwent a heat
319 shock treatment at 37°C for 40 minutes. Larvae were then transferred to a 25°C incubator
320 where they remained until eclosion.

321 **Data and Software Availability**

322 The data discussed in this publication have been deposited in NCBI's Gene Expression
323 Omnibus and are accessible through GEO series accession number GEO: GSE308165
324 (https://www.ncbi.nlm.nih.gov/geo/query/acc.cgi?acc=GSE308165)

325 **Regrowth quantification**

326 To quantify regrowth, we used a method first described in a previous publication
327 (Bornstein et al., 2021) and illustrated in Figure 6. Two reference lines were extended:
328 line y (red), representing the full length of the γ-lobe (determined based on FasII staining),
329 and line x (yellow), indicating the extent of clonal γ-axon regrowth (determined as the
330 most distal point the axons reach). The regrowth index was calculated as the ratio of x to
331 y (x/y), providing a normalized measure of axonal regrowth.

332 Statistical analyses for regrowth quantification were performed in R. Proportional data
333 were logit-transformed prior to testing to meet assumptions of normality and homogeneity

334 of variance. Group differences were evaluated using one-way ANOVA, followed by
335 Dunnett's post hoc test comparing all groups to Pmvk. A significant difference was
336 detected only between control and *Pmvk*^{E20*} ($p < 0.001$). Significance levels are indicated
337 in the figures as *** for $p < 0.001$.
338

339 **Results**

340 **Lineage-related neuronal types in the *Drosophila* mushroom body undergo intial**
341 **axon growth and developmental regrowth in similar spatiotemporal conditions**

342 In a previous study (Alyagor et al., 2018), we found that the developmental age was by
343 far the most dominant factor in defining the transcriptional profile of γ-KCs, something
344 that was later confirmed also in developing projection neurons (PNs, Xie et al 2021 – from
345 Luo lab). Remarkably, adult γ-KCs were more similar, on a global level, to other adult
346 neurons than to larval or pupal γ-KCs. Notably, while initial axon growth occurs in
347 embyonic and early larval life, developmental regrowth occurs during metamorphosis.
348 Therefore, to reliably compare the genetic programs of initial axon growth and
349 developmental regrowth, we sought to profile two similar neuronal types that undergo
350 different axon growth states at the same developmental window. The lineage-related α/β-
351 and γ-KCs were a perfect match, as within a similar timeframe during the pupal stage,
352 α/β-KCs extend their axons for the first time, while γ-KCs regrow their axons after pruning
353 (Figure 1A-B).

354 To achieve our goal, we screened for drivers that would specifically label α/β-KCs at the
355 pupal stage, when they send out axonal processes. We therefore screened 30 Gal4 driver
356 lines considered to be α/β-specific in adult flies (Supplementary table 1), and imaged
357 them at 6 and 24 h APF. To our surprise, only one line - R16B01-Gal4 - was specific to
358 the MB (i.e., not expressed elsewhere in the brain), and within the MB, specific to α/β-
359 KCs throughout their growth (Figure 1C). At 18 h APF, α/β-KCs labeled with R16B01-Gal4
360 showed cell bodies with short, loosely arranged axons that were still difficult to follow. By
361 21 h APF, these axons had gathered into a tight bundle, and their growing axon tips were
362 visible. Observations throughout the pupal stage revealed that these axons extended and
363 reached the tips of the lobes by 36 hours APF (Figure 1C).

364 Identifying this driver enabled us to isolate α/β-KCs throughout their initial axon growth.
365 For comparative purposes, we also repeated the isolation and profiling of γ-KCs, as
366 previously done in our lab (Alyagor et al., 2018), using the same driver (R71G10-Gal4)
367 that specifically labels developing γ-KCs (Figure 1D). Labeling both types of neurons gave
368 us the opportunity to isolate and sequence each population while they extend their axons

369 for the first (α/β) or second (γ) time. Altogether, we sorted and sequenced α/β- and γ-KCs
370 at 5 pupal timepoints - every three hours from 18 h until 30 h APF - in addition to adult.
371 We used Principal Component Analysis (PCA) to compare the transcriptional profiles of
372 developing and adult α/β- and γ-KCs. Our results confirmed our prior knowledge (Alyagor
373 et al., 2018) that adult γ- or α/β-KCs are more similar to each other than to their own devel
374 opmental forms. Notably, developing γ- and α/β-KCs occupied a specific region in the
375 PCA space (Figure 1E).

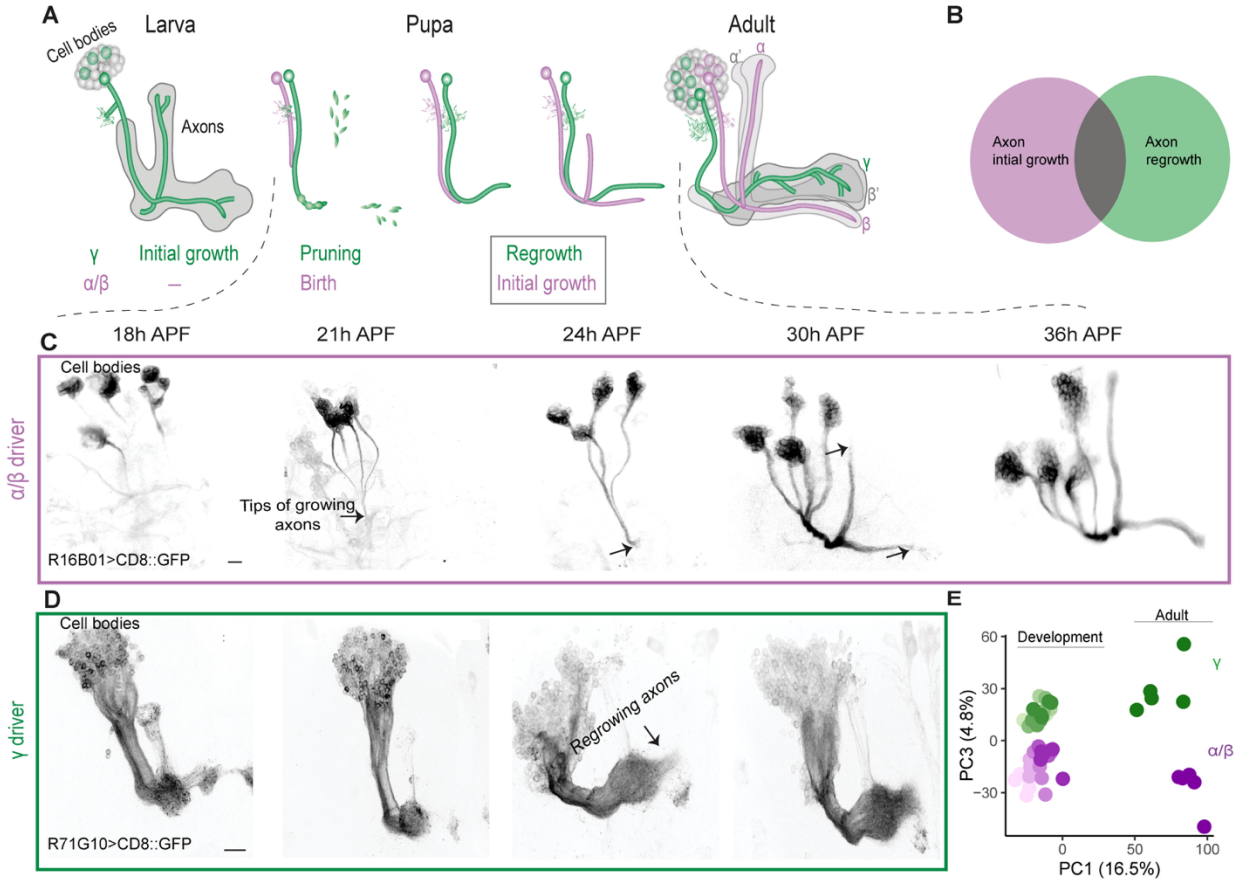

376

377 **Figure 1. Lineage-related neuronal types undergo intial axon growth and regrowth**
378 **in shared spatiotemporal conditions.** (A) A model of MB development highlighting that
379 the regrowth of γ-axons temporally and spatially overlaps with the initial growth of α/β-
380 axons.
381 (B) A Venn diagram depicting the theoretical and predicted comparison between α/β initial
382 axon growth and γ-axon regrowth.
383 (C) Confocal Z-projections of R16B01-Gal4 driving membranal GFP expression
384 (mCD8::GFP), which specifically labels developing α/β-KCs during the pupal stage. The
385 images were captured at five time points between 18h until 36h APF, when the axons
386 reach the end of the lobes. At 18h APF, four groups of cell bodies can be observed,

corresponding to newly born cells from the four neuroblasts, each sending out short axons that progressively extend in each subsequent image. The axon tips are marked with arrows.
(D) Confocal Z-projections of γ-KCs labeled with R71G10-Gal4 driving mCD8::GFP expression, as identified by (Alyagor et al., 2018), between 18h to 30h APF. At 21 hours APF, the axons are completely pruned and begin to re-extend for a second time. By 24 hours APF, the regrowing axons are visible (arrow).
(E) PCA of α/β and γ-KC expression profiles during development and in adult. Color code depicts neuronal type (green for γ and magenta for α/β) and developmental stage (from light to dark as development progresses).

Comparative transcriptomic analysis of α/β-axon initial growth and γ-axon regrowth reveals common and unique molecular players

Our bulk smart-seq2 (see materials and methods) dataset includes reads from 8,222 distinct genes expressed in at least in one cell type across (γ and/or α/β) six developmental time points. To identify developmentally-regulated patterns of gene expression, we first analyzed the expression profiles of α/β-KCs. We thus concentrated on 3,345 genes that demonstrated dynamic expression in α/β-KCs, i.e., showed statistically significant differential expression during at least one developmental timepoint compared to adult. k-means clustering of those α/β-KC dynamic expression patterns resulted in eight distinct clusters with unique developmental expression profiles (see materials and methods). For example, genes in clusters 1 and 2 are upregulated during the pupal stage but show decreased expression in adults, and thus potentially include activators of axon growth (Figure 2A). In contrast, genes in cluster 5 are downregulated during the pupal stage, followed by increased expression in adults, suggesting these are mostly adult specific genes. Gene Ontology (GO) term analysis further supports this observation. Cluster 1 is enriched for genes involved in axon development and other key developmental processes, including Toll pathway signaling, cytoskeletal rearrangement, and PTEN regulation. In contrast, cluster 5 is enriched for genes associated with synaptic transmission as well as learning and memory (Figure S2).

As α/β clusters 1+2 include the best candidates for axon growth promoters, but contain a large number of genes (1142 genes; Figure 2A, C), we sought to narrow down the list of candidates. Since we aimed to identify genes required for axon growth in both neuronal

420 types, we decided focus on genes within α/β clusters 1+2, and examine their expression
421 in the γ-KC dataset. We therefore re-clustered the 1,162 genes in α/β clusters 1+2 based
422 on their transcriptional expression in γ-KCs (Figure 2B): cluster 1 was subdivided into
423 clusters 1A-1J, while cluster 2 was subvidided into 2A-2G. To identify shared genes
424 required for both the initial growth of α/β-axons and the regrowth of γ-axons (Figure 2B–
425 C), we focused on the first three sub-clusters in each heatmap (clusters 1A-C; 2A-C), as
426 they are comprised of genes that are upregulated during axon growth of both neuronal
427 types. From these six clusters, we compiled a set of 676 genes, out of which we selected
428 a subset of 300 genes, which are strongly upregulated during axon growth and are
429 associated with biologically relevant functions based on GO term analysis and have tools
430 to perturb their function (namely – flies expressing RNAi targeting these specific genes).
431 Genes primarily associated with processes less directly related to axon growth—such as
432 cell cycle regulation, DNA replication, chromosome organization, chromatin remodeling,
433 and ribosomal structure—were excluded from further analysis.

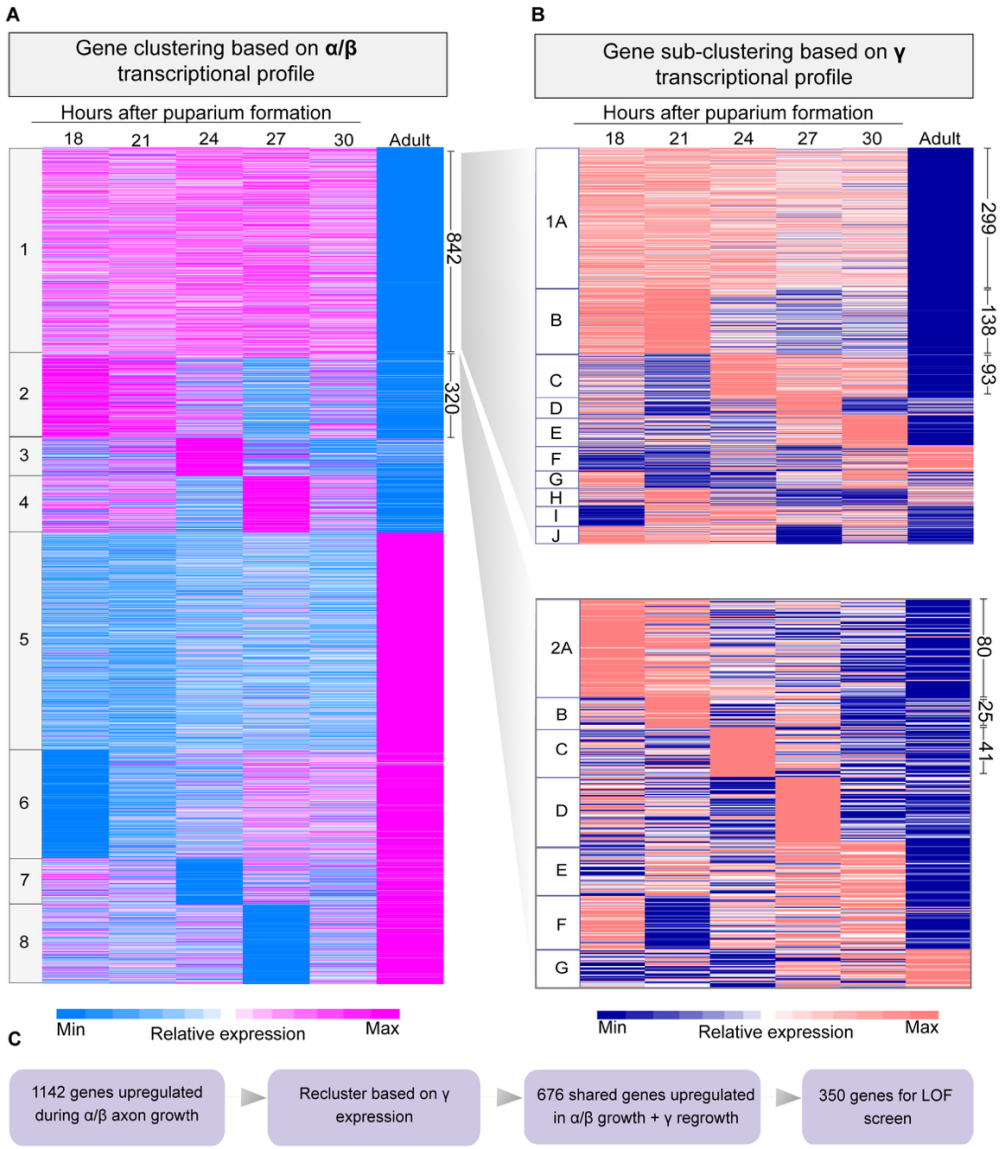

Figure 2. Comparative transcriptomic analysis of α/β-axon initial growth and γ-axon regrowth. (A) Heatmap showing k-means clustering of 3345 differentially expressed genes during α/β-KC development. Light blue and magenta represent low and high relative expression, respectively.

(B) Heatmaps showing k-means re-clustering of 842 genes from cluster 1 or 320 genes from cluster 2 based on the γ-KC transcriptional profiling. Blue and coral represent low and high relative expression, respectively.

For all the heatmaps, each horizontal line describes the relative expression of a single gene. Gene expression was determined in five timepoints after pupa formation (18, 21, 24, 27 and 30 hours APF) and in adult. The number of genes within selected clusters are specified to the right.

(C) A flow chart detailing the criteria used to select candidate genes for the loss-of-function (LOF) screen.

448 **RNAi-based screen identifies 12 genes that are essential for γ- and/or α/β-axon**
449 **morphology**
450 For the loss-of-function screen, we employed an RNAi-mediated knockdown (KD)
451 strategy, where we expressed RNAi species targeting candidate genes using the OK107-
452 Gal4 driver (which is strongly expressed in all KC types - γ, α'/β' and α/β). γ-axons were
453 visualized in adult brains using a second, independent binary system, via expression of
454 myristylated tandem Tomato (mtdT) driven by R71G10-QF2 – which consistently labels
455 γ-KCs and stochastically labels α/β-KCs (Figure 3). Due to this stochasticity, we
456 additionally stained the brains with anti-Fasciclin II (FasII) antibody, which strongly labels
457 α/β-axons (and weakly labels γ-axons, but never α'/β'-axons).
458 Out of the 300 genes we screened, KD of 40 genes resulted in various morphological and
459 structural defects (such as thinner axonal lobes, axon misguidance, and branching
460 abnormalities), 12 of which showed axonal defects – which we categorized into three
461 phenotypic groups (Figure 3): defects in γ-axons but normal α/β-axons (Figure 3C-F);
462 defects in both α/β- and γ-axons (Figure 3G-O); and normal γ-axons but no visible α/β
463 axons (Figure 3P-Q). In addition to the axonal phenotypes that are categorized in Figure
464 3, KD of several of these 12 genes additionaly resulted in additional defects, such as
465 altered number and shape of cell bodies (data not shown). Notably, 7 of the 12 genes
466 identified in the screen are involved in protein maturation, encompassing post-
467 translational modifications such as folding, cleavage, and prenylation.

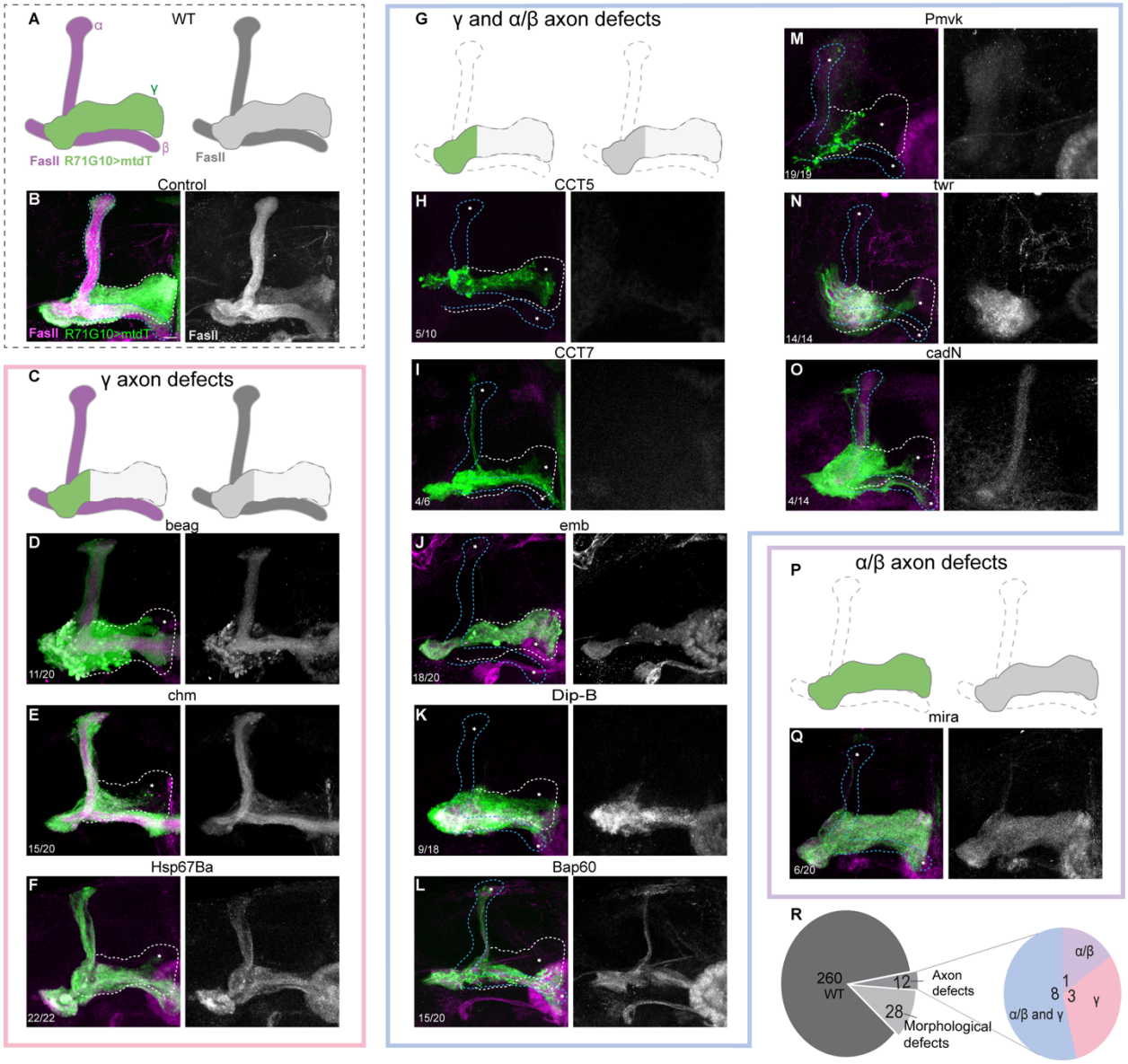

Figure 3. RNAi-based screen identifies 12 genes that are essential for γ- and/or α/β-axon morphology. (A) Schematic of the WT α/β- and γ-axonal lobes, illustrating labeling patterns that match the corresponding confocal images. γ-axons are labeled in green using mtdT:3xHA under the control of R71G10-QF2. FasII is visualized with antibody staining shown in magenta, and also presented separately in greyscale.

(B) Confocal Z-projection of a control MB in which γ-KCs are labeled by mtdT:3xHA (green) driven by R71G10-QF2, and OK107-Gal4 drives the expression of Luciferase. Magenta (left panel) or greyscale (right panel) is anti-FasII staining, which strongly labels α/β-axons and weakly labels γ-axons.

(C,G,P) Schematics of α/β- and/or γ-axon lobe defects.

(D-F,H-O,Q) Confocal Z-projections of adult MBs in which γ-KCs are labeled by mtdT:3xHA (green) driven by R71G10-QF2, with OK107-Gal4 driving expression of RNAi

481 targeting beag (beag; D); chameau (chm; E); Heat shock gene 67Ba (Hsp67Ba; F);
482 Chaperonin containing TCP1 subunit 5 (CCT5; H); Chaperonin containing TCP1 subunit
483 7 (CCT7; I); embargoed (emb; J); Dipeptidase B (Dip-B; K); Brahma associated protein
484 60kD (Bap60; L); Phosphomevalonate kinase (Pmvk; M); twisted bristles roughened eye
485 (twr; N); cadherin-N (cadN; O); miranda (mira; Q).
486 (R) Pie charts showing the phenotypic distribution of the 300 screened genes (left), and
487 of the axon growth phenotypes of the 12 'positive hits' (right).
488 The putative WT γ- and α/β-lobes are outlined in white and blue, respectively. Asterisks
489 mark the missing part of α/β or γ lobes. Frame colors in (C-Q) represent the phenotypic
490 group as depicted in (R). Numbers represent the fraction of MBs displaying the presented
491 phenotype. Scale bar is 10 μm.
492

493 **Pmvk, cadN and twr are cell-autonomously required for γ-axon regrowth**

494 To inspect the KD phenotypes at better resolution, as well as gain information regarding
495 cell-autonomous requirement, we silenced the genes specifically within neuroblast (NB)
496 clones using the mosaic analysis with a repressible cell marker (MARCM) technique (Lee
497 and Luo, 1999). We used the OK107-Gal4 pan-KC driver, resulting in NB clones in which
498 all KC types are labeled as well as express the relevant RNAi. To our surprise, we
499 observed that only Pmvk, cadN and twr showed severe defects in γ-axon regrowth (Figure
500 S3E-G), while the others exhibited γ lobes that were either WT-like, or showed weak
501 regrowth defects (Figure S3). For mira KD, which we expected to affect α/β growth, the
502 lobes seemed to form normally (Figure S3M). In the case of emb, CCT5, and CCT7, the
503 neuroblast clones included only γ-, but no α/β- or α'/β'-KCs (Figure S3B-D), most likely
504 due to a proliferation defect of the neuroblast, which prevented it from generating later
505 born neurons.
506 The proliferation defects in the emb, CCT5 and CCT7 NB clones might suggest that the
507 lack of α/β axons upon KD in the entire population of neurons (Figure 3) is because the
508 neurons were never born, rather than a *bona fida* axon growth defect. To more specifically
509 examine the role of these three candidate genes in α/β-axon growth, we selectively
510 silenced emb, CCT5 and CCT7 in α/β-KCs by inducing MARCM clones at the third instar
511 larval stage (L3; Figure S4) - a time in which only α/β KCs are born (Lee and Luo, 1999).
512 Only single cell clones were visible, suggesting cell-lethality or severe proliferation
513 defects. Importantly, all α/β single-cell clones exhibited WT-like axonal growth (Figure

514 S4), indeed suggesting that the axonal defects observed in Figure 3 are due to non-cell-
515 autonomous effects.
516 Taken together, our findings indicate that Pmvk, cadN, and twr are cell-autonomously
517 required for γ-axon regrowth. For the purpose of this study, we chose to focus on Pmvk,
518 although cadN and twr remain compelling candidates for future investigation.

519 **Pmvk is cell autonomously required for γ-axon regrowth but not for initial axon**
520 **extension of γ- nor α/β-KCs**

521 To further investigate the role of Pmvk in axon growth during development, we specifcially
522 silenced it in γ-KCs using the γ-specific driver R71G10-Gal4. We found that while γ-axons
523 extended normally during the larval stage (L3; Figure 4A-B), the medial γ-lobe failed to
524 fully regrow as evident in the adult stage (Figure 4C-D). To determine whether Pmvk is
525 also required for α/β-axon growth, we silenced it using the R44E04-Gal4 driver (of note,
526 R44E04-Gal4 is strongly expressed in α/β throughout development but also transienty in
527 α'/β' and in non-MB neurons, which was the reason it was not chosen for the RNA profiling
528 experiment; data not shown). In contrast to the γ-axons, α/β-axons showed no detectable
529 defects following Pmvk KD (Figure 4E-F).
530 We next used CRISPR/Cas9 to generate a novel Pmvk mutant allele - $Pmvk^{E20}$ - which
531 carries a single-nucleotide substitution resulting in a premature stop codon at amino acid
532 20 (Figure 4M). Due to its homozygous lethality, we analyzed this mutant allele in MARCM
533 clones. In $Pmvk^{E20}$ single-cell γ clones, initial axon growth appeared normal (Figure 4G-
534 H), but, as expected, axons failed to regrow following pruning (Figure 4I-J). In contrast to
535 γ-axons, and in accordance with the RNAi KD results, α/β neuroblast $Pmvk^{E20}$ clones
536 displayed normal axon elongation (Figure 4K-L). Notably, Pmvk mutants produced no NB
537 clones, suggesting an additional requirement for Pmvk in neuroblast proliferation or cell
538 survival.
539

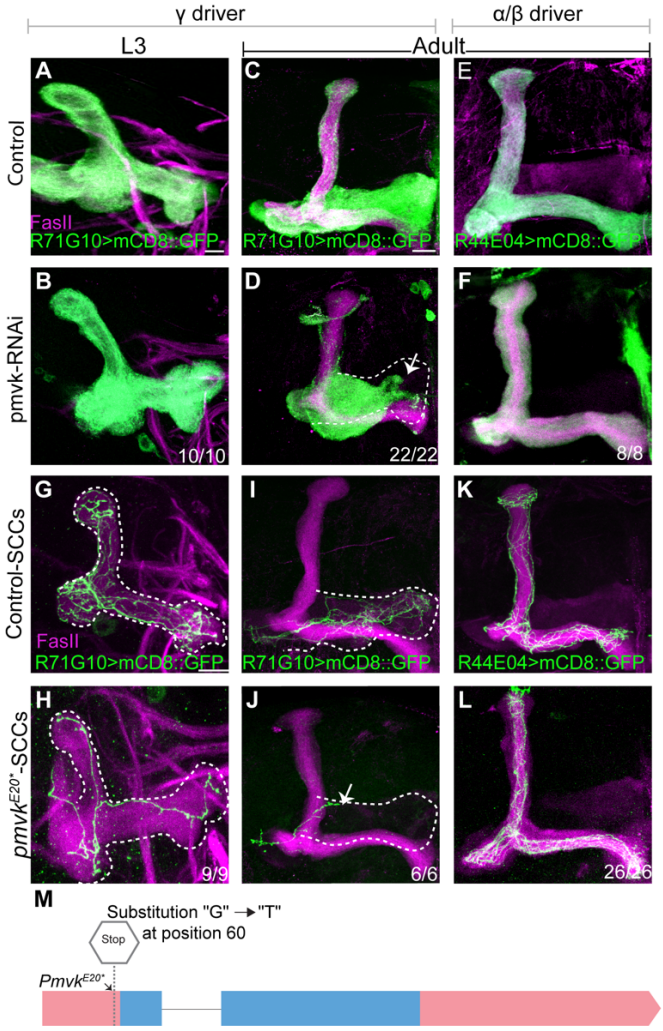

Figure 4. Pmvk is cell autonomously required for γ-axon regrowth but not for initial axon extension of γ nor α/β. (A-F) Confocal Z-projections of L3 (A-B) or adult (C-F) MBs with γ-KCs labeled by mCD8::GFP (green) driven by the γ-specific R71G10-Gal4 (A-D), or the α/β-specific R44E04-Gal4 (E-F). MBs in images (B-F) also express RNAi targeting Pmvk driven by R71G10-Gal4 (B,D) or R44E04-Gal4 (F) .

(G-L) Confocal z-projections of control (G,I,K) or *Pmvk*^{E20*} (H,J,L) MARCM clones in L3 (G-H) or Adult (I-L). R71G10-Gal4 (G-J) or R44E04-Gal4 (K-L) drive expression of mCD8::GFP (green). The clone was generated by heat-shocking @24 hours after egg-laying (G-J) or @L3 (K-L).

The full extent of the γ lobe in adult (as determined by the FasII channel) and L3 is outlined in white. Magenta is FasII staining. Arrows demarcate axon growth defects. Scale bar is 10 μm for all except G,where it represents 20 μm. Numbers represent the fraction of MBs displaying the presented phenotype.

(M) Schematic representation of the *Pmvk*^{E20*} mutant allele, which includes a single-nucleotide substitution (G>T) at position 60, corresponding to amino acid 20, leading to the replacement of glutamic acid (E) with a stop codon.

557 **The mevalonate pathway is essential for γ-axon regrowth**

558 Pmvk is part of the mevalonate pathway – a highly conserved metabolic enzymatic
559 pathway that consumes acetyl coenzyme A to synthesize a wide variety of isoprenoids,
560 such as cholesterol, dolichol, isopentenyl tRNA, and ubiquinone (Figure 5D; Edwards and
561 Ericsson, 2025; Hinson et al., 1997). We knocked down the additional seven key enzymes
562 in the pathway and found that pan-KC silencing of either hmgcr or mvk led to seemingly
563 similar γ-regrowth defects (but not defects in α/β extension; Figure 5A-C), suggesting an
564 overall requirement of the mevalonate pathway for γ-axon regrowth.

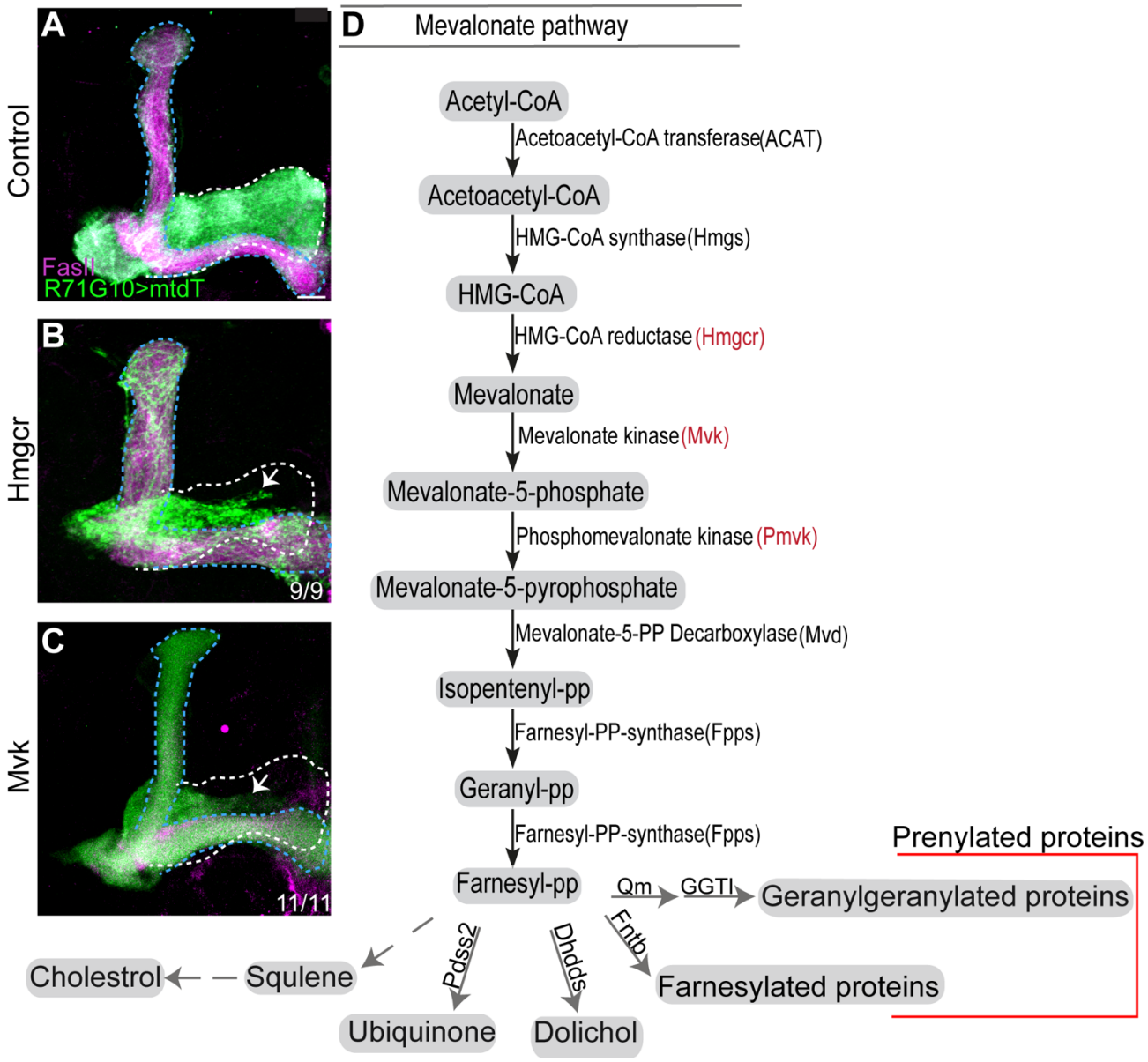

565

566

Figure 5. The mevalonate pathway is essential for γ-axon regrowth. (A-C) Confocal Z-projections of adult MBs from control (A) or those expressing RNAi targeting hmgcr (B) or mvk (C) driven by the pan-KC driver OK107-Gal4. γ-KCs are labeled by mtdT:3xHA (green) driven by R71G10-QF2. Magenta is FasII staining. The putative WT γ- and α/β-lobes are outlined in white and blue, respectively. Arrows indicate axon growth defects. Numbers represent the fraction of MBs displaying the presented phenotype. Scale bar is 10 μm.
(D) A schematic of the mevalonate pathway, illustrating key metabolites and enzymes. Enzymes shown in red are those found to influence γ-axon development. The diagram also highlights the different downstream routes that FPP can take—either toward the synthesis of sterol isoprenoids (e.g., cholesterol) or non-sterol isoprenoids (such as ubiquinone, dolichol, and isopentenyl-tRNA). Additionally, FPP serves as a precursor for protein prenylation, which occurs in two main forms: farnesylation and geranylgeranylation. The dashed arrows emphasize that cholesterol biosynthesis is absent in *Drosophila*.

Pmvk likely regulates axon regrowth via the TOR pathway

The mevalonate pathway generates a common isoprenoid product that can be directed into five major downstream pathways. In mammals, one of these is cholesterol biosynthesis, which is absent in *Drosophila* (emphasized with in dashed arrows-Figure 5D*)*; instead, flies must obtain cholesterol from their diet (Cesur et al., 2023). The other four branches are: (2) ubiquinone synthesis, (3) dolichol synthesis, and (4–5) protein prenylation, through the addition of either farnesyl (4) or geranylgeranyl (5) groups. Prenylation increases protein hydrophobicity, thereby regulating their association with cellular membranes and influencing their function.

To test which of these branches might contribute to axon regrowth, we knocked down the major enzymes required for each process. However, none of these manipulations produced a regrowth defect (Figure S5). This could be due to insufficient efficiency of RNAi KD, or because simultaneous KD of two or more enzymes is necessary to reveal an effect. Since we were unable to pinpoint a specific downstream pathway, we decided to focus on the prenylation branch, as it was previously shown that prenylated proteins, such as the Rho GTPase and Rheb (Ras homolog enriched in brain), are associated with axon growth (Ng and Luo, 2004; Hall and Lalli, 2010).

Importantly, previous work from our lab demonstrated that the nuclear receptor unfulfilled (UNF) promotes axon regrowth by activating a program mediated, at least in part, by the

602 Rheb-TOR-S6 kinase pathway (Figure 6A; Yaniv et al., 2012). We thus conducted rescue
603 experiments in Pmvk mutants by overexpressing Rho, Rheb, and more importantly - a
604 constitutively active variant of the Rheb downstream effector S6 kinase ($S6K^{CA}$).
605 Overexpression of Rho within Pmvk mutant clones showed no suppressive effect on the
606 regrowth defect (Fig. 6B,E). Rheb overexpression did not significantly rescue γ-axon
607 regrowth in the Pmvk mutant background (3/7 clones; Fig. 6B,F), which is consistent with
608 the requirement for prenylation to achieve full Rheb activity and TOR activation. In
609 contrast, $S6K^{CA}$ overexpression showed a clearer trend toward suppression of the
610 regrowth defect (6/10 clones displaying near-complete γ-axon extension; Fig. 6B,G).
611 However, this effect did not reach statistical significance with the current sample size, and
612 unfortunately we were unable to further increase n (see acknowledgements). Taken
613 together, these results suggest that Pmvk promotes γ-axon regrowth through the Rheb–
614 TOR pathway.
615
616
617

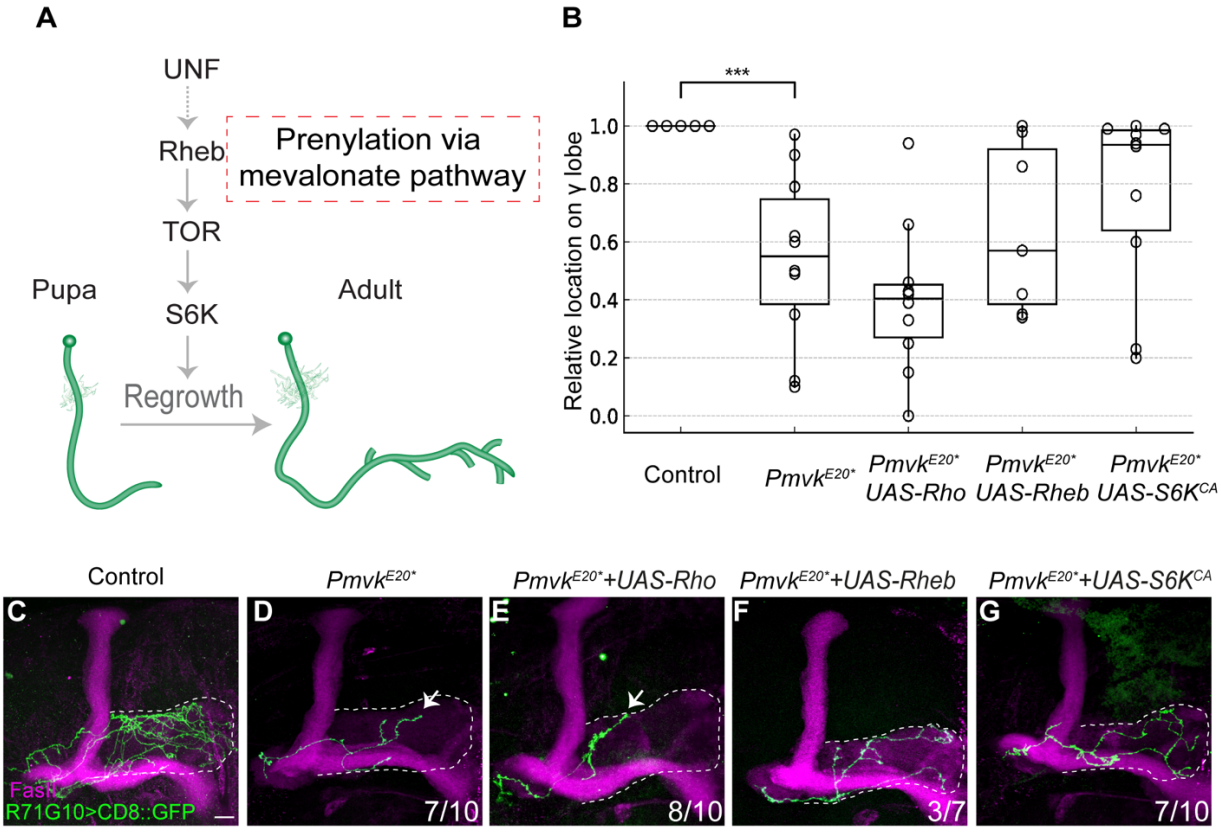

618

Figure 6. Pmvk likely regulates axon regrowth via the TOR pathway
(A) Scheme of developing γ-KCs in which UNF promotes regrowth via the TOR pathway (adapted from Yaniv et al., 2012). Rheb is a CAAX protein that undergoes prenylation, enabling its translocation to the plasma membrane to activate downstream effectors.
(B) Quantification of axon regrowth for the genotypes displayed in (C-G). The x/y ratio indicates relative axon position along the adult γ lobe (quantification described in Figure S7). Box plots represent the median (line), interquartile range (box), and spread within 1.5×IQR (whiskers), circles indicate individual data points. Groups were compared using one-way ANOVA on logit-transformed data followed by Tukey's HSD. A significant difference was observed only between control and $Pmvk^{E20*}$ (***$p < 0.001$). Comparisons of $Pmvk^{E20*}$ with $Pmvk^{E20*}$ and UAS-Rho ($p = 0.696$), or UAS-Rheb ($p = 0.704$), or *UAS-S6K*^{CA} ($p = 0.120$) were not significant.
(C-G) Confocal Z-projections of γ single-cell MARCM clones in adult MBs, either control (C, comprised of multiple single cell clones), $Pmvk^{E20*}$ homozygous mutant (D), or $Pmvk^{E20*}$ homozygous mutant also overexpressing Rho (E), Rheb (F) or *S6K*^{CA} (G).
The γ-specific driver R71G10-Gal4 drives expression of membranal GFP (mCD8::GFP; green). Magenta is FasII staining. The γ lobe is outlined by a dashed white line. Arrows indicate axon growth defects. Numbers represent the fraction of MBs displaying the presented phenotype. Scale bar is 10 μm.

Discussion

How axon growth is regulated across different cellular and developmental contexts remains largely unknown. In this study, we used the remodeling MB as a model to uncover the transcriptional profiles of two lineage-related neuron types - γ- and α/β-KCs - which undergo developmental axon regrowth and initial axon growth, respectively, in similar spatiotemporal conditions. By comparing their transcriptional programs, we identified shared and unique expression patterns, highlighting candidates for an RNAi screen through which we identified genes promoting γ- and/or α/β-axon formation. One gene we found to be essential for regrowth of γ-axons is Pmvk, an enzyme in the mevalonate pathway responsible for isoprenoid biosynthesis. While Pmvk has not previously been linked to axon growth, isoprenoids are known to be required for the prenylation of small GTPases such as RhoA, Ras, and Cdc42—key regulators of the cytoskeleton and axon guidance (Hakeda-Suzuki et al., 2002; Hall and Lalli, 2010; Lee et al., 2021; Ng and Luo, 2004). Our findings suggest that Pmvk contributes to axon regrowth at least in part by supporting the membrane localization of Rheb, a prenylation-dependent GTPase previously shown to promote γ-axon regrowth (Yaniv et al., 2012).

655 A major strength of this study lies in its high temporal resolution, enabled by RNA-seq
656 analysis across five developmental stages (at 3-hour intervals) plus adulthood. This was
657 enabled due to a Gal4 line that we characterized and found that it is specific to α/β-KCs
658 throughout development, which allowed us to capture α/β-KCs during active. Notably, our
659 screening approach was aimed at uncovering shared genes required for both α/β growth
660 and γ regrwth. However, despite identifying several γ regrowth-promoting genes, our
661 screen did not uncover any strong candidates cell-autonomously required for α/β axon
662 growth. This may reflect the robustness and/or redundancy of the genetic programs
663 controlling α/β development, where the loss of individual genes might be buffered by
664 compensatory pathways. Previous studies suggested that larval γ axons provide a
665 structural template for later-born KC types, including α/β-neurons, which otherwise follow
666 a relatively stereotyped and stable developmental trajectory (Kurusu et al., 2002). Most
667 of the genes known to affect α/β-KC development, such as FasII, Drl, and Netrin, impact
668 guidance, branching, or stability but not necessarily initial axon extension (Bates et al.,
669 2014; Fushima and Tsujimura, 2007; Hatch et al., 2021; Kang et al., 2019; Lin et al., 2009;
670 Reynaud et al., 2015). One exception is twinstar (tsr), which encodes Cofilin and is
671 required for early α/β axon growth, highlighting actin regulation as a potential neuron-
672 intrinsic vulnerability in these cells (Ng and Luo, 2004). Similarly, Sickie was shown to be
673 required for early α/β growth, functioning through a non-canonical Rac–Cofilin pathway
674 (Abe et al., 2014). Notably, even in these cases a scenario of normal initial growth
675 followed by late developmental axonal degeneration has not been directly ruled out. Our
676 findings suggest that combinatorial loss-of-function experiments, or temporally-targeted
677 approaches, may be necessary to uncover additional regulators of α/β initial growth.
678 Our data provide a valuable resource for the *Drosophila* neuroscience community,
679 particularly given that γ- and α/β-KCs together constitute the majority of the intrinsic MB
680 neurons. The identification of Pmvk as a growth-promoting factor opens new avenues for
681 dissecting how metabolic processes shape axonal remodeling. Since Pmvk is involved in
682 isoprenoid synthesis required for protein prenylation, its role likely intersects with the
683 activity of small GTPases such as Rheb, which are essential for growth signaling. This
684 suggests a model in which metabolic enzymes like Pmvk act upstream to facilitate the
685 activation of growth-promoting pathways through post-translational modification of key

686 signaling molecules. Understanding this link between metabolism and signaling may shed
687 light on how neurons integrate internal metabolic states with external developmental cues
688 to regulate growth.
689 The broader role of the mevalonate pathway in axon growth is complex and context-
690 dependent. While some studies have shown that inhibiting this pathway impairs axon
691 extension, others suggest it may promote regeneration under certain conditions (Li et al.,
692 2016; Schulz et al., 2004). This may reflect the dual role of the pathway in both isoprenoid
693 and cholesterol synthesis. Pharmacological inhibition of the pathway aimed at reducing
694 cholesterol levels —as with the widely used statins, which directly inhibit hmgcr, the rate-
695 limiting enzyme of the mevalonate pathway—could thus potentially have unintended
696 effects on neuronal growth. Moreover, this pathway is tightly regulated by nutrient-
697 sensitive signals, including insulin and TOR signaling (Belgacem and Martin, 2007), which
698 activate SREBP, a transcription factor controlling lipid metabolism regulators like hmgcr.
699 In *Drosophila*, SREBP is known to regulate lipid homeostasis and may influence neuronal
700 remodeling through the mevalonate pathway (Seegmiller et al., 2002). Together, our
701 findings highlight a critical link between cellular metabolism, signaling, and axon growth,
702 suggesting that a neuron's ability to remodel relies on sustained metabolic support and
703 coordination between growth and nutrient-sensing pathways.
704 Finally, understanding axon growth capacity is key for regeneration after injury. Our
705 transcriptomic and genetic analyses point to candidate genes for testing in repair. Future
706 efforts to injure γ-axons and compare their injury-evoked transcriptional program with
707 those of initial α/β growth and developmental γ regrowth could provide valuable insights
708 into shared and regeneration-specific molecular pathways.
709

710 **Acknowledgements**

711 We thank the Bloomington Drosophila Stock Center and the Vienna Drosophila Resource
712 Center for providing fly stocks. Monoclonal antibodies were obtained from the
713 Developmental Studies Hybridoma Bank, created under the auspices of the NICHD and
714 maintained by the University of Iowa. We are grateful to D. Robbins and to the staff of the
715 Crown Institute for Genomics, INCPM for performing the RNA-seq, and to E. Hagai for
716 assistance with cell sorting. This work was supported by the Minerva Foundation (grant

714145) with funding from the Federal German Ministry of Education and Research, the Samowitz Foundation Trust, the Estate of Gerald Alexander, and by the European Research Council (ERC) Advanced Grant #101054886, “NeuRemodelBehavior”. O.S. is the incumbent of the Prof. Erwin Netter Professorial Chair of Cell Biology.

On June 15, 2025, our laboratory was directly hit by an Iranian missile and was completely destroyed, which unfortunately currently limits our ability to increase sample size (Figure 6) and to provide the Pmvk mutant allele generated in this study (which we are now in the process of rebuilding it).

References

Abe, T., Yamazaki, D., Murakami, S., Hiroi, M., Nitta, Y., Maeyama, Y., Tabata, T., 2014. The NAV2 homolog Sickie regulates F-actin-mediated axonal growth in Drosophila mushroom body neurons via the non-canonical Rac-Cofilin pathway. Development 141, 4716–4728. https://doi.org/10.1242/dev.113308

Alyagor, I., Berkun, V., Keren-Shaul, H., Marmor-Kollet, N., David, E., Mayseless, O., Issman-Zecharya, N., Amit, I., Schuldiner, O., 2018. Combining Developmental and Perturbation-Seq Uncovers Transcriptional Modules Orchestrating Neuronal Remodeling. Dev. Cell 47, 38-52.e6. https://doi.org/10.1016/j.devcel.2018.09.013

Aso, Y., Grübel, K., Busch, S., Friedrich, A.B., Siwanowicz, I., and, H.T., 2009. The Mushroom Body of Adult Drosophila Characterized by GAL4 Drivers. J. Neurogenet. 23, 156–172. https://doi.org/10.1080/01677060802471718

Aso, Y., Hattori, D., Yu, Y., Johnston, R.M., Iyer, N.A., Ngo, T.-T., Dionne, H., Abbott, L., Axel, R., Tanimoto, H., Rubin, G.M., 2014. The neuronal architecture of the mushroom body provides a logic for associative learning. eLife 3, e04577. https://doi.org/10.7554/eLife.04577

Bates, K.E., Sung, C., Hilson, L., Robinow, S., 2014. unfulfilled Interacting Genes Display Branch-Specific Roles in the Development of Mushroom Body Axons in Drosophila melanogaster. G3 GenesGenomesGenetics 4, 693–706. https://doi.org/10.1534/g3.113.009829

Belgacem, Y.H., Martin, J.-R., 2007. Hmgcr in the Corpus Allatum Controls Sexual Dimorphism of Locomotor Activity and Body Size via the Insulin Pathway in Drosophila. PLOS ONE 2, 1–11. https://doi.org/10.1371/journal.pone.0000187

Belle, J.S.D., Heisenberg, M., 1994. Associative odor learning in Drosophila abolished by chemical ablation of mushroom bodies. Science. https://doi.org/10.1126/science.8303280

Bornstein, B., Meltzer, H., Adler, R., Alyagor, I., Berkun, V., Cummings, G., Reh, F., Keren-Shaul, H., David, E., Riemensperger, T., Schuldiner, O., 2021. Transneuronal Dpr12/DIP-δ interactions facilitate compartmentalized dopaminergic innervation of Drosophila mushroom body axons. EMBO J. 40, e105763. https://doi.org/10.15252/embj.2020105763

Bornstein, B., Zahavi, E.E., Gelley, S., Zoosman, M., Yaniv, S.P., Fuchs, O., Porat, Z., Perlson, E., Schuldiner, O., 2015. Developmental Axon Pruning Requires Destabilization of Cell Adhesion by JNK Signaling. Neuron 88, 926–940. https://doi.org/10.1016/j.neuron.2015.10.023

Cesur, M.F., Basile, A., Patil, K.R., Çakır, T., 2023. A new metabolic model of Drosophila melanogaster and the integrative analysis of Parkinson's disease. Life Sci. Alliance 6, e202201695. https://doi.org/10.26508/lsa.202201695

Dobin, A., Davis, C.A., Schlesinger, F., Drenkow, J., Zaleski, C., Jha, S., Batut, P., Chaisson, M., Gingeras, T.R., 2013. STAR: ultrafast universal RNA-seq aligner. Bioinformatics 29, 15–21. https://doi.org/10.1093/bioinformatics/bts635

Edwards, P.A., Ericsson, J., 2025. STEROLS AND ISOPRENOIDS: SIGNALING MOLECULES DERIVED FROM THE CHOLESTEROL BIOSYNTHETIC PATHWAY.

Fushima, K., Tsujimura, H., 2007. Precise control of fasciclin II expression is required for adult mushroom body development in Drosophila. Dev. Growth Differ. 49, 215–227. https://doi.org/10.1111/j.1440-169X.2007.00922.x

Hakeda-Suzuki, S., Ng, J., Tzu, J., Dietzl, G., Sun, Y., Harms, M., Nardine, T., Luo, L., Dickson, B.J., 2002. Rac function and regulation during Drosophila development. Nature 416, 438–442. https://doi.org/10.1038/416438a

Hall, A., Lalli, G., 2010. Rho and Ras GTPases in Axon Growth, Guidance, and Branching. Cold Spring Harb. Perspect. Biol. 2, a001818–a001818. https://doi.org/10.1101/cshperspect.a001818

Hatch, H.A., Belalcazar, H.M., Marshall, O.J., Secombe, J., 2021. A KDM5–Prospero transcriptional axis functions during early neurodevelopment to regulate mushroom body formation. eLife 10, e63886. https://doi.org/10.7554/eLife.63886

Hilton, B.J., Husch, A., Schaffran, B., Lin, T., Burnside, E.R., Dupraz, S., Schelski, M., Kim, J., Müller, J.A., Schoch, S., Imig, C., Brose, N., Bradke, F., 2022. An active vesicle priming machinery suppresses axon regeneration upon adult CNS injury. Neuron 110, 51-69.e7. https://doi.org/10.1016/j.neuron.2021.10.007

Hinson, D.D., Chambliss, K.L., Toth, M.J., Tanaka, R.D., Gibson, K.M., 1997. Post-translational regulation of mevalonate kinase by intermediates of the cholesterol and nonsterol isoprene biosynthetic pathways. J. Lipid Res. 38, 2216–2223. https://doi.org/10.1016/S0022-2275(20)34935-X

Horton, J.D., Goldstein, J.L., Brown, M.S., 2002. SREBPs: activators of the complete program of cholesterol and fatty acid synthesis in the liver. J. Clin. Invest. 109, 1125–1131. https://doi.org/10.1172/JCI15593

Jenett, A., Rubin, G.M., Ngo, T.-T.B., Shepherd, D., Murphy, C., Dionne, H., Pfeiffer, B.D., Cavallaro, A., Hall, D., Jeter, J., Iyer, N., Fetter, D., Hausenfluck, J.H., Peng, H., Trautman, E.T., Svirskas, R.R., Myers, E.W., Iwinski, Z.R., Aso, Y., DePasquale, G.M., Enos, A., Hulamm, P., Lam, S.C.B., Li, H.-H., Laverty, T.R., Long, F., Qu, L., Murphy, S.D., Rokicki, K., Safford, T., Shaw, K., Simpson, J.H., Sowell, A., Tae, S., Yu, Y., Zugates, C.T., 2012. A GAL4-Driver Line Resource for Drosophila Neurobiology. Cell Rep. 2, 991–1001. https://doi.org/10.1016/j.celrep.2012.09.011

803 Kang, H., Zhao, J., Jiang, X., Li, G., Huang, W., Cheng, H., Duan, R., 2019. Drosophila
804 Netrin-B controls mushroom body axon extension and regulates courtship-
805 associated learning and memory of a Drosophila fragile X syndrome model. Mol.
806 Brain 12, 52. https://doi.org/10.1186/s13041-019-0472-1
807 Kurusu, M., Awasaki, T., Masuda-Nakagawa, L.M., Kawauchi, H., Ito, K., Furukubo-
808 Tokunaga, K., 2002. Embryonic and larval development of the Drosophila
809 mushroom bodies: concentric layer subdivisions and the role of fasciclin II.
810 Development 129, 409–419. https://doi.org/10.1242/dev.129.2.409
811 Lee, S.J., Zdradzinski, M.D., Sahoo, P.K., Kar, A.N., Patel, P., Kawaguchi, R., Aguilar,
812 B.J., Lantz, K.D., McCain, C.R., Coppola, G., Lu, Q., Twiss, J.L., 2021. Selective
813 axonal translation of the mRNA isoform encoding prenylated Cdc42 supports
814 axon growth. J. Cell Sci. 134, jcs251967. https://doi.org/10.1242/jcs.251967
815 Lee, T., Lee, A., Luo, L., 1999a. Development of the Drosophila mushroom bodies:
816 Sequential generation of three distinct types of neurons from a neuroblast.
817 Development 126, 4065–4076.
818 Lee, T., Lee, A., Luo, L., 1999b. Development of the Drosophila mushroom bodies:
819 Sequential generation of three distinct types of neurons from a neuroblast.
820 Development 126, 4065–4076.
821 Lee, T., Luo, L., 1999. Mosaic analysis with a repressible neurotechnique cell marker for
822 studies of gene function in neuronal morphogenesis. Neuron.
823 https://doi.org/10.1016/S0896-6273(00)80701-1
824 Lee, T., Marticke, S., Sung, C., Robinow, S., Luo, L., 2000. Cell-autonomous
825 requirement of the USP/EcR-B ecdysone receptor for mushroom body neuronal
826 remodeling in Drosophila. Neuron 28, 807–818. https://doi.org/10.1016/S0896-
827 6273(00)00155-0
828 Li, H., Kuwajima, T., Oakley, D., Nikulina, E., Hou, J., Yang, W.S., Lowry, E.R., Lamas,
829 N.J., Amoroso, M.W., Croft, G.F., Hosur, R., Wichterle, H., Sebti, S., Filbin, M.T.,
830 Stockwell, B., Henderson, C.E., 2016. Protein Prenylation Constitutes an
831 Endogenous Brake on Axonal Growth. Cell Rep. 16, 545–558.
832 https://doi.org/10.1016/j.celrep.2016.06.013
833 Lin, S., Huang, Y., Lee, T., 2009. Nuclear Receptor Unfulfilled Regulates Axonal
834 Guidance and Cell Identity of Drosophila Mushroom Body Neurons. PLOS ONE
835 4, 1–12. https://doi.org/10.1371/journal.pone.0008392
836 Lindner, J., Dassa, B., Wigoda, N., Stelzer, G., Feldmesser, E., Prilusky, J., Leshkowitz,
837 D., 2025. UTAP2: an enhanced user-friendly transcriptome and epigenome
838 analysis pipeline. BMC Bioinformatics 26, 79. https://doi.org/10.1186/s12859-
839 025-06090-8
840 Love, M.I., Huber, W., Anders, S., 2014. Moderated estimation of fold change and
841 dispersion for RNA-seq data with DESeq2. Genome Biol. 15, 550.
842 https://doi.org/10.1186/s13059-014-0550-8
843 Marmor-Kollet, N., Schuldiner, O., 2016. Contrasting developmental axon regrowth and
844 neurite sprouting of Drosophila mushroom body neurons reveals shared and
845 unique molecular mechanisms. Dev. Neurobiol. 76, 262–276.
846 https://doi.org/10.1002/dneu.22312

Ng, J., Luo, L., 2004. Rho GTPases Regulate Axon Growth through Convergent and Divergent Signaling Pathways. Neuron 44, 779–793. https://doi.org/10.1016/j.neuron.2004.11.014

Picelli, S., Faridani, O.R., Björklund, Å.K., Winberg, G., Sagasser, S., Sandberg, R., 2014. Full-length RNA-seq from single cells using Smart-seq2. Nat. Protoc. 9, 171–181. https://doi.org/10.1038/nprot.2014.006

Qian, C., Zhou, F.-Q., 2020. Updates and challenges of axon regeneration in the mammalian central nervous system. J. Mol. Cell Biol. 12, 798–806. https://doi.org/10.1093/jmcb/mjaa026

Rabinovich, D., Yaniv, S.P., Alyagor, I., Schuldiner, O., 2016. Nitric Oxide as a Switching Mechanism between Axon Degeneration and Regrowth during Developmental Remodeling. Cell 164, 170–182. https://doi.org/10.1016/j.cell.2015.11.047

Reynaud, E., Lahaye, L.L., Boulanger, A., Petrova, I.M., Marquilly, C., Flandre, A., Martianez, T., Privat, M., Noordermeer, J.N., Fradkin, L.G., Dura, J.-M., 2015. Guidance of Drosophila Mushroom Body Axons Depends upon DRL-Wnt Receptor Cleavage in the Brain Dorsomedial Lineage Precursors. Cell Rep. 11, 1293–1304. https://doi.org/10.1016/j.celrep.2015.04.035

Rozo, J.A., Martínez-Gallego, I., Rodríguez-Moreno, A., 2024. Cajal, the neuronal theory and the idea of brain plasticity. Front. Neuroanat. 18. https://doi.org/10.3389/fnana.2024.1331666

Schuldiner, O., Yaron, A., 2015. Mechanisms of developmental neurite pruning. Cell. Mol. Life Sci. 72, 101–119. https://doi.org/10.1007/s00018-014-1729-6

Schulz, J.G., Bösel, J., Stoeckel, M., Megow, D., Dirnagl, U., Endres, M., 2004. HMG-CoA reductase inhibition causes neurite loss by interfering with geranylgeranylpyrophosphate synthesis. J. Neurochem. 89, 24–32. https://doi.org/10.1046/j.1471-4159.2003.02305.x

Seegmiller, A.C., Dobrosotskaya, I., Goldstein, J.L., Ho, Y.K., Brown, M.S., Rawson, R.B., 2002. The SREBP Pathway in Drosophila: Regulation by Palmitate, Not Sterols. Dev. Cell 2, 229–238. https://doi.org/10.1016/S1534-5807(01)00119-8

Sudarsanam, S., Yaniv, S., Meltzer, H., Schuldiner, O., 2020. Cofilin regulates axon growth and branching of Drosophila γ-neurons. J. Cell Sci. 133. https://doi.org/10.1242/jcs.232595

Sutherland, T.C., Geoffroy, C.G., 2020. The Influence of Neuron-Extrinsic Factors and Aging on Injury Progression and Axonal Repair in the Central Nervous System. Front. Cell Dev. Biol. Volume 8-2020. https://doi.org/10.3389/fcell.2020.00190

Tirian, L., Dickson, B.J., 2017. The VT GAL4, LexA, and split-GAL4 driver line collections for targeted expression in the Drosophila nervous system. bioRxiv 198648. https://doi.org/10.1101/198648

Yaniv, S.P., Issman-Zecharya, N., Oren-Suissa, M., Podbilewicz, B., Schuldiner, O., 2012. Axon regrowth during development and regeneration following injury share molecular mechanisms. Curr. Biol. 22, 1774–1782. https://doi.org/10.1016/j.cub.2012.07.044

Yaniv, S.P., Meltzer, H., Alyagor, I., Schuldiner, O., 2020. Developmental axon regrowth and primary neuron sprouting utilize distinct actin elongation factors. J. Cell Biol. 219. https://doi.org/10.1083/jcb.201903181

Zhou, Y., Zhou, B., Pache, L., Chang, M., Khodabakhshi, A.H., Tanaseichuk, O., Benner, C., Chanda, S.K., 2019. Metascape provides a biologist-oriented resource for the analysis of systems-level datasets. Nat. Commun. 10, 1523. https://doi.org/10.1038/s41467-019-09234-6